Title	Compact dual-mode triple-band bandpass filters using three pairs of degenerate modes in a ring resonator
Author(s)	Luo, S; Zhu, L; Sun, S
Citation	IEEE Transactions on Microwave Theory And Techniques, 2011, v. 59 n. 5, p. 1222-1229
Issued Date	2011
URL	http://hdl.handle.net/10722/139261
Rights	IEEE Transactions on Microwave Theory and Techniques. Copyright © IEEE

Compact Dual-Mode Triple-Band Bandpass Filters Using Three Pairs of Degenerate Modes in a Ring Resonator

Sha Luo, *Student Member, IEEE*, Lei Zhu, *Senior Member, IEEE*, and Sheng Sun, *Member, IEEE*

***Abstract*—In this paper, a class of triple-band bandpass filters with two transmission poles in each passband is proposed using three pairs of degenerate modes in a ring resonator. In order to provide a physical insight into the resonance movements, the equivalent lumped circuits are firstly developed, where two transmission poles in the first and third passbands can be distinctly tracked as a function of port separation angle. Under the choice of 135° and 45° port separations along a ring, four open-circuited stubs are attached symmetrically along the ring and they are treated as perturbation elements to split the two second-order degenerate modes, resulting in a two-pole second passband. To verify the proposed design concept, two filter prototypes on a single microstrip ring resonator are finally designed, fabricated, and measured. The three pairs of transmission poles are achieved in all three passbands, as demonstrated and verified in simulated and measured results.**

***Index Terms*—Bandpass filter, dual mode, open-circuited stubs, ring resonator, triple band.**

I. Introduction

TRIPLE-BAND transceivers have shown their potential in modern multiband wireless communication systems [1], [2]. As an important circuit block, the triple-band bandpass filters have garnered a lot of attention over the past few years. In a typical design, two different resonators are used to realize the desired three passbands [3]–[6]. The first and third passbands are realized by the first and second resonant modes of either stepped-impedance resonator (SIR) [3], [4] or stub-loaded resonators [5], [6]. The second passband is created by the first resonant mode of an additional resonator. In all these studies, four resonators were employed to complete their final designs. The works in [7]–[10] tried to demonstrate that a triple-band bandpass filter can be designed using a tri-section SIR or stub-loaded resonator. However, at least two identical resonators need to be used together in order to create two transmission poles in each passband. There are some other methods that are also developed for the design of triple passband filters with the three passband in close proximity, such as the dual behavior resonator (DBR) [11], parallel coupling topology [12], coupling-matrix method [13], inverter-coupled resonator [14], frequency transformation [15], and band-splitting technique [16]. However, to the best of our knowledge, all the triple-band bandpass filters developed thus far require at least two resonators, regardless of varied frequency spacing between the triple passbands.

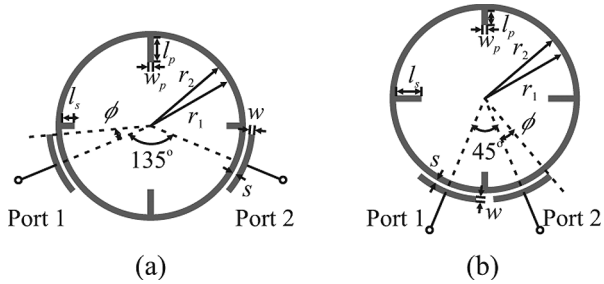

Fig. 1. Schematics of the proposed ring resonators with two distinct port excitation angles (2θ). (a) 135°. (b) 45°.

Very recently, a single ring resonator was applied to develop compact dual-mode dual-band bandpass filters [17]–[19]. In [17], the two ports were positioned at 135° separation. The two pairs of the first- and third-order degenerate modes of a ring were excited under strong capacitive coupling between a ring resonator and two ports, thus making up the two operating passbands. An alternative dual-mode dual-band bandpass filter was later designed by using the first- and second-order degenerate modes of a ring resonator where the two ports are separated by 135° [18] and 45° [19], respectively.

The main objective of this work is to extend our design concept in [17]–[19] toward the theoretical design and practical exploration of a class of compact triple-band bandpass filters using three pairs of degenerate modes in a single ring resonator. First, an equivalent lumped circuit is developed under even- and odd-mode excitations to provide physical insight into the movements of two pairs of first- and third-order resonant modes as a function of port separation angle. In our design, the two-port excitation angle is set to be 135° or 45° such that the second passband is fully suppressed for a uniform ring at the beginning. As the four open-circuited stubs are introduced as perturbation elements, the second passband is created with two transmission poles. Fig. 1(a) and (b) shows the schematics of the two proposed ring resonators with an excitation angle of 135° and 45°. After their operating principle is described, the two dual-mode triple-band bandpass filters on a single ring resonator are finally

Manuscript received September 09, 2010; revised February 18, 2011; accepted February 25, 2011. Date of publication April 05, 2011; date of current version May 11, 2011.

S. Luo and L. Zhu are with the School of Electrical and Electronic Engineering, Nanyang Technological University, Singapore 639798 (e-mail: luos0002@ntu.edu.sg; ezhul@ntu.edu.sg).

S. Sun is with the School of Electrical and Electronic Engineering, The University of Hong Kong, Pokfulam, Hong Kong (e-mail: sunsheng@ieee.org).

Color versions of one or more of the figures in this paper are available online at http://ieeexplore.ieee.org.

Digital Object Identifier 10.1109/TMTT.2011.2123106

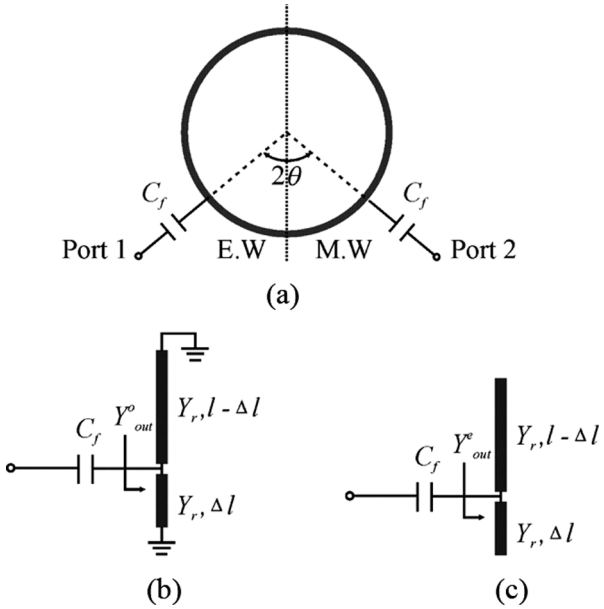

Fig. 2. (a) Schematic of a uniform ring resonator capacitively excited via capacitors at a separation angle (2θ) between two ports. (b) Odd-mode one-port bisection. (c) Even-mode one-port bisection.

designed, fabricated, and measured. The good agreement between the simulated and measured results verifies the proposed design principle.

II. Dual-Modes in First and Third Resonances

Fig. 2(a) depicts the schematic of a uniform ring resonator that is excited by two identical capacitors (C_f) at a separation angle (2θ) between two excitation ports. Under odd- or even-mode excitation at the two ports, the symmetrical plane in Fig. 2(a) becomes a perfect electric wall (E.W.) or magnetic wall (M. W.). Fig. 2(b) and (c) show the transmission-line models of the two one-port bisection networks, where the short- and open-circuited ends represent the E.W. and M.W., respectively. Y_r is the characteristic admittance of the ring, l is equal to half of the length of the ring, and Δl represents the length from the feeding point to the symmetric plane of the ring.

Under odd-mode excitation, the output admittance of the one-port network looking into the right side after C_f is

$$\begin{aligned} Y^o_{\text{out}} &= -jY_r\left[\frac{1}{\tan(\beta\Delta l)} + \frac{1}{\tan\beta(l-\Delta l)}\right] \\ &= jY_r\frac{2\sin\beta l}{\cos\beta l - \cos\beta(l-2\Delta l)}. \end{aligned} \tag{1}$$

Similarly, the output admittance under even-mode excitation can be obtained

$$\begin{aligned} Y^e_{\text{out}} &= jY_r[\tan(\beta\Delta l) + \tan\beta(l-\Delta l)] \\ &= jY_r\frac{2\sin\beta l}{\cos\beta l + \cos\beta(l-2\Delta l)}. \end{aligned} \tag{2}$$

At the first resonance with an angular frequency ω_{10}, $\beta l = \pi(180^\circ)$ and $\beta\Delta l = \theta$. The angular frequency near ω_{10} can be reasonably expressed as $\omega = \omega_{10} + \Delta\omega$, when $\Delta\omega$ is very small. Thus, the admittances in (1) and (2) can be simplified as

$$Y^o_{\text{out}} \approx jY_r\frac{-2\pi\Delta\omega/\omega_{10}}{-1+\cos(2\theta)} = jY_r\frac{\Delta\omega\pi}{\sin^2\theta\omega_{10}} \tag{3}$$

and

$$Y^e_{\text{out}} \approx jY_r\frac{-2\pi\Delta\omega/\omega_{10}}{-1-\cos(2\theta)} = jY_r\frac{\Delta\omega\pi}{\cos^2\theta\omega_{10}}. \tag{4}$$

Similarly, at the third resonance ω_{30}, $\beta l = 3\pi(540^\circ)$ and $\beta\Delta l = 3\theta$. The angular frequency near ω_{30} is $\omega = \omega_{30} + \Delta\omega$, when $\Delta\omega$ is small, such that we have

$$Y^o_{\text{out}} \approx jY_r\frac{-6\pi\Delta\omega/\omega_{30}}{-1+\cos(6\theta)} = jY_r\frac{3\Delta\omega\pi}{\sin^2 3\theta\omega_{30}} \tag{5}$$

and

$$Y^e_{\text{out}} \approx jY_r\frac{-6\pi\Delta\omega/\omega_{30}}{-1-\cos(6\theta)} = jY_r\frac{3\Delta\omega\pi}{\cos^2 3\theta\omega_{30}}. \tag{6}$$

On the other hand, for the parallel *LC* resonator circuit in Fig. 3(a), its input admittance around resonance can be derived as

$$Y_{\text{in}} = 2j\Delta\omega C \tag{7}$$

where $L = 1/\omega_0^2 C$ and ω_0 is the angular resonant frequency. Comparing (3)–(6) with (7), we can find that the parallel *LC* circuits can be used to represent half of a symmetrical bisection of a ring resonator under odd- and even-mode excitations around its first and third resonances. Given the equivalence of Figs. 2(b) and 3(a), the odd-mode equivalent capacitance and inductance around the first resonance are derived as

$$C_{1o} = \frac{Y_r\pi}{2\sin^2\theta\omega_{10}} \tag{8a}$$

$$L_{1o} = \frac{2\sin^2\theta}{Y_r\pi\omega_{10}}. \tag{8b}$$

Meanwhile, the even-mode equivalent capacitance and inductance near the first resonance are

$$C_{1e} = \frac{Y_r\pi}{2\cos^2\theta\omega_{10}} \tag{9a}$$

$$L_{1e} = \frac{2\cos^2\theta}{Y_r\pi\omega_{10}}. \tag{9b}$$

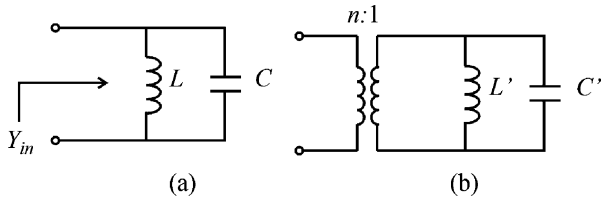

Fig. 3. (a) Parallel *LC* resonator. (b) Equivalent circuit of one-port bisections in Fig. 2(b) and (c) that consists of a transformer and a parallel *LC* resonator.

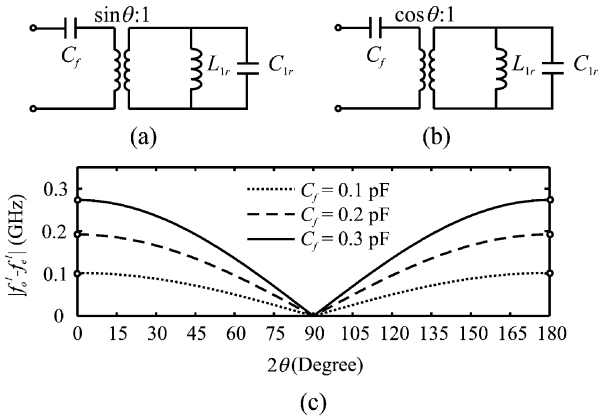

Fig. 4. (a) Odd-mode equivalent lumped circuits. (b) Even-mode equivalent lumped circuits. (c) Spacing between two transmission poles around the first resonance (2.56 GHz) under varied external capacitors (C_f) with $Y_r = 1/82\ \Omega^{-1}$.

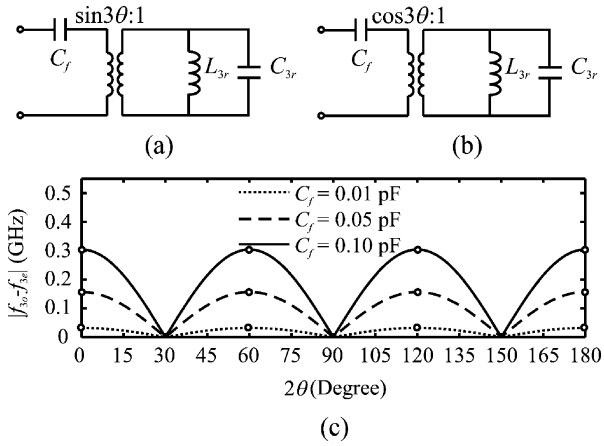

Fig. 5. (a) Odd-mode equivalent lumped circuits. (b) Even-mode equivalent lumped circuits. (c) Spacing between two transmission poles around the third resonance (7.68 GHz) under varied external capacitors (C_f) with $Y_r = 1/82\ \Omega^{-1}$.

Similarly, around the third resonance, these equivalent capacitances and inductances under odd- and even-mode excitations are

$$C_{3o} = \frac{3Y_r\pi}{2\sin^2 3\theta\omega_{30}} \tag{10a}$$

$$L_{3o} = \frac{2\sin^2 3\theta}{3Y_r\pi\omega_{30}} \tag{10b}$$

$$C_{3e} = \frac{3Y_r\pi}{2\cos^2 3\theta\omega_{30}} \tag{11a}$$

$$L_{3e} = \frac{2\cos^2 3\theta}{3Y_r\pi\omega_{30}}. \tag{11b}$$

Notice that the capacitors and inductors in (8a)–(11b) are all dependent on the separation angle (θ). Thus, a simple, but general, *LC* resonator in Fig. 3(a) is modified to an alternative circuit shown in Fig. 3(b), where a transformer with the turns ratio of $n:1$ is placed before the *LC* resonator with L' and C'.

Around the first resonance, n is equal to $\sin\theta$ and $\cos\theta$ for the odd- and even-mode excitations. Thus, the transmission-line models in Fig. 2(b) and (c) can be simplified as those lumped-circuit models shown in Fig. 4(a) and (b), respectively, with the capacitance and inductance given by

$$C_{1r} = \frac{Y_r\pi}{2\omega_{10}} \tag{12a}$$

$$L_{1r} = \frac{2}{Y_r\pi\omega_{10}}. \tag{12b}$$

Furthermore, the odd- and even-mode resonant angular frequencies around the first resonance are calculated as

$$\omega_{1o} = \frac{1}{\sqrt{L_{1r}(C_{1r} + \sin^2\theta C_f)}} \tag{13a}$$

$$\omega_{1e} = \frac{1}{\sqrt{L_{1r}(C_{1r} + \cos^2\theta C_f)}} \tag{13b}$$

where $\cos\theta \neq 0$ or $\sin\theta \neq 0$. From the transmission-line models in Fig. 2(b) and (c), it is easy to understand that, if $\sin\theta = 0$, only odd-mode resonance is excited; if $\cos\theta = 0$, only even-mode resonance is excited. When $2\theta = 90°$, the odd- and even-mode circuits resonate at the same frequency. It confirms that only one pole appears at the first resonance of an uniform ring resonator with a port-separation angle (2θ) of 180° or 90°, as discussed in [20]. Fig. 4(c) demonstrates how the odd- and even-mode resonant frequencies (f_{1o} and f_{1e}) merge together as 2θ moves from 0° to 90° and how they split again as 2θ changes from 90° to 180°. Of course, these two resonant frequencies also depend on the capacitance (C_f). With the same port separation angle (2θ), the bigger C_f is, the further apart the two frequencies are. Using the same method, the equivalent circuit for the third resonance can be derived as shown in Fig. 5(a) and (b), respectively, where

$$C_{3r} = \frac{3Y_r\pi}{2\omega_{30}} \tag{14a}$$

$$L_{3r} = \frac{2}{3Y_r\pi\omega_{30}}. \tag{14b}$$

The third-order odd- and even-mode resonances occurs at

$$\omega_{3o} = \frac{1}{\sqrt{L_{3r}(C_{3r} + \sin^2 3\theta C_f)}} \tag{15a}$$

$$\omega_{3e} = \frac{1}{\sqrt{L_{3r}(C_{3r} + \cos^2 3\theta C_f)}} \tag{15b}$$

where $\cos 3\theta \neq 0$ or $\sin 3\theta \neq 0$. Looking at Figs. 4(c) and 5(c), we can figure out that the spacing between the two resonant frequencies, $|f_{3o} - f_{3e}|$, around the third resonance varies much more significantly than that around the first resonance. In particular, we find that the odd- and even-mode circuits resonate at the same frequency if $2\theta = 30°$, 90°, and 150° are selected. Moreover, the spacing between these odd- and even-mode resonant frequencies can be enlarged by increasing the value of C_f.

Tables I and II tabulate the two sets of transmission poles around the first and third resonances, which are calculated from (13a) and (13b) and (15a) and (15b) with respect to Fig. 2(a). Good agreement with each other is observed. In addition, when $2\theta = 135°$ and 45°, the two degenerate modes around both the

TABLE I
CALCULATED AND SIMULATED POLES AROUND THE FIRST RESONANCE (2.56 GHz) WITH $Y_r = 1/82\ \Omega^{-1}$

C_f= 0.1 pF

2θ	15°	45°	75°	105°	135°
Calculated Poles (GHz)	2.465/2.563	2.478/2.549	2.500/2.526	2.500/2.526	2.478/2.549
Simulated Poles (GHz)	2.465/2.563	2.479/2.549	2.502/2.523	2.498/2.526	2.476/2.550

C_f= 0.3 pF

2θ	15°	45°	75°	105°	135°
Calculated Poles (GHz)	2.296/2.559	2.327/2.519	2.383/2.453	2.383/2.453	2.327/2.519
Simulated Poles (GHz)	2.310/2.559	2.351/2.512	2.422/2.422	2.384/2.452	2.323/2.520

TABLE II
CALCULATED AND SIMULATED POLES AROUND THE THIRD RESONANCE (7.68 GHz) WITH $Y_r = 1/82\ \Omega^{-1}$

C_f= 0.01 pF

2θ	15°	45°	75°	105°	135°
Calculated Poles (GHz)	7.664 / 7.687				
Simulated Poles (GHz)	7.668/7.690	7.667/7.690	7.668/7.690	7.667/7.690	7.667/7.690

C_f= 0.1 pF

2θ	15°	45°	75°	105°	135°
Calculated Poles (GHz)	7.430 / 7.645				
Simulated Poles (GHz)	7.478/7.640	7.423/7.652	7.467/7.643	7.433/7.450	7.455/7.646

first and third resonances of a ring resonator are excited at the different frequencies.

III. DUAL MODES IN SECOND RESONANCE

Our next step is to investigate the excitation of two degenerate modes at the second resonance of the ring resonator. At ω_{20}, $\beta l = 2\pi(360°)$ and $\beta\Delta l = 2\theta$. For an angular frequency $\omega = \omega_{20} + \Delta\omega$, when $\Delta\omega$ is small, we have

$$Y_{\text{out}}^{o} \approx jY_r \frac{-4\pi\Delta\omega/\omega_{20}}{-1+\cos(4\theta)} = jY_r \frac{2\Delta\omega\pi}{\sin^2 2\theta\omega_{20}} \tag{16}$$

and

$$Y_{\text{out}}^{e} \approx jY_r \frac{-4\pi\Delta\omega/\omega_{20}}{-1-\cos(4\theta)} = jY_r \frac{2\Delta\omega\pi}{\cos^2 2\theta\omega_{20}}. \tag{17}$$

Similarly, equivalent odd- and even-mode lumped circuits around ω_{20} can be also expressed in terms of Fig. 6(a) and (b), where

$$C_{2r} = \frac{Y_r\pi}{\omega_{20}} \tag{18a}$$

$$L_{2r} = \frac{1}{Y_r\pi\omega_{20}}. \tag{18b}$$

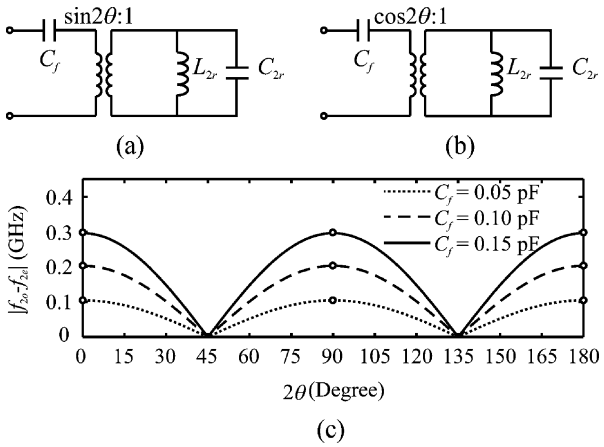

Fig. 6. (a) Odd-mode equivalent lumped circuits. (b) Even-mode equivalent lumped circuits. (c) Spacing between two transmission poles around the second resonance (5.13 GHz) under varied external capacitors (C_f) with $Y_r = 1/82\ \Omega^{-1}$.

In this way, the second-order odd- and even-mode resonant angular frequencies can be calculated as

$$\omega_{2o} = \frac{1}{\sqrt{L_{2r}(C_{2r}+\sin^2 2\theta C_f)}} \tag{19a}$$

$$\omega_{2e} = \frac{1}{\sqrt{L_{2r}(C_{2r}+\cos^2 2\theta C_f)}} \tag{19b}$$

where $\cos 2\theta \neq 0$ or $\sin 2\theta \neq 0$. Fig. 6(c) gives three sets of spacings between two resonant frequencies or transmission poles, i.e., $|f_{2o} - f_{2e}|$, under varied external capacitance C_f. The results in Fig. 6(c) illustrate that the spacing between two poles or resonant frequencies reaches its peak at $2\theta = 90°$ and becomes zero at $2\theta = 135°$ and $45°$. As discussed above, the port-to-port excitation angle (2θ) needs to be selected as 135° or 45° in order to suppress the second resonance of a ring resonator, but, in this case, the odd- and even-mode resonant frequencies merge to the same frequency at $2\theta = 135°$ and $45°$, as shown in Fig. 6(c).

Using the perturbation methodology in the design of traditional dual-mode ring bandpass filters, e.g., [20], four open-circuited stubs are attached symmetrically with the ring resonator, as shown in Fig. 7(a). They are introduced herein as perturbation elements in order to split the two second-order degenerate modes while giving infinitesimal influence on the spacing between the two degenerate modes at the first and third resonances. In Fig. 7(a), Z_r is the characteristic impedance of the ring and open-circuited stubs, θ_r is the electrical length of one quarter of the ring, θ_p is the electrical length of the two vertical stubs, and θ_s is the electrical length of the two horizontal stubs.

As shown in Fig. 7(b) and (c), at the second-order odd- and even-mode resonances, one quadrant of the whole ring resonator act as half-wavelength short and open resonator, respectively. With reference to Fig. 7(b) and (c), the odd- and even-mode resonant conditions can be derived based on the well-known transverse resonance method, where

$$\tan\theta_r = 0 \tag{20a}$$

$$\tan\theta_r = \frac{2(\tan\theta_s + \tan\theta_p)}{\tan\theta_s\tan\theta_p - 4}. \tag{20b}$$

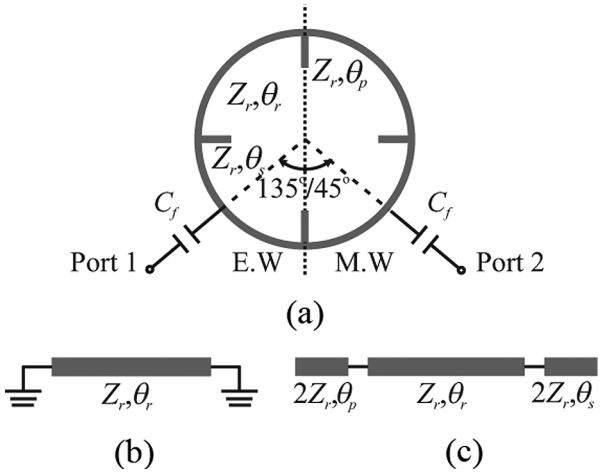

Fig. 7. (a) Stub-loaded ring resonator with two lumped-capacitors at the excitation positions. (b) and (c) Equivalent quadrant-ring models at second-order odd- and even-mode resonances.

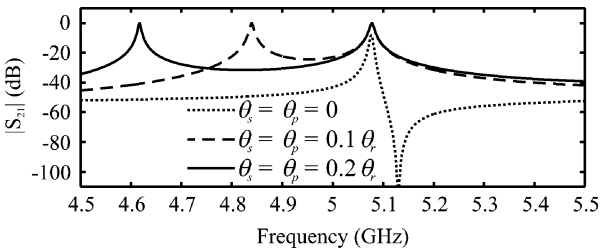

Fig. 8. Frequency responses around the second resonance of a ring resonator with the strip width of 0.3 mm versus varied stub lengths (θ_s and θ_p) under week coupling at two ports ($C_f = 0.05$ pF).

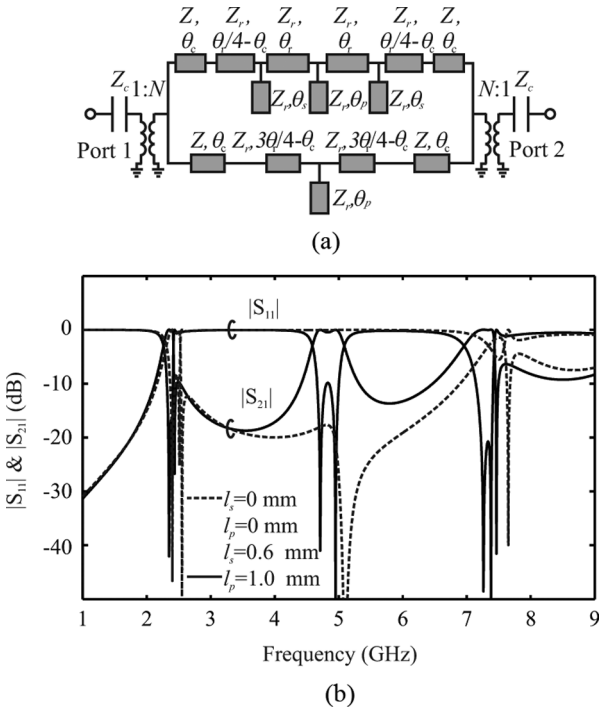

Fig. 9. (a) Equivalent model of the ring circuit in Fig. 1(a). (b) Theoretical frequency responses for varied stub lengths (l_p and l_s) ($r_1 = 7.03$ mm, $r_2 = 7.33$ mm, $w_p = 0.30$ mm, $s = 0.10$ mm, and $\theta_c = 4\theta_r/9$. Substrate: $\epsilon_r = 10.8$, $h = 1.27$ mm).

It can be immediately understood from (20a) and (20b) that the addition of four stubs only affects the even-mode resonant frequencies while having no influence on their odd-mode one. Fig. 8 illustrates the splitting of the two second-order resonant frequencies for a ring circuit in Fig. 7(a) with a separation angle of $2\theta = 135°$. With no stubs installed in the ring, i.e., $\theta_s = \theta_p = 0$, the two resonant frequencies become the same as each other and they are both equal to 5.08 GHz. As the electrical length $(\theta_s = \theta_p)$ of the four identical stubs increases to $0.1\theta_r$ and $0.2\theta_r$, the even-mode resonant frequency (f_e) decreases to 4.84 and 4.62 GHz, while its odd-mode resonant frequency (f_o) remains at 5.08 GHz. Thus far, we have demonstrated that the two second-order degenerate modes of a ring resonator with the 130° or 45° port-to-port separation angle can be also split by introducing these four stubs as perturbation structures.

IV. Two Triple-Band Filters: Design and Results

Based on the detailed discussion in Sections II and III, two triple-band microstrip-ring-resonator bandpass filters can be constructed using three pairs of degenerate modes occurring at ω_{10}, ω_{20}, and ω_{30}. In order to simplify the design, uniform ring resonators are used for filter design to prove our design principle. Fig. 1(a) and (b) displays the schematics of the two proposed ring-resonator filters with the port-to-port separation angle $2\theta = 135°$ and 45°, respectively, where r_1 and r_2 stand for the inner and outer radii of the ring. The ring is capacitively coupled with the two feed lines via two identical parallel-coupled lines with the coupling angle of 2Φ, coupling gap of s, and strip width of $w = r_2 - r_1$. The width of four stubs is set to w_p, whereas the lengths of the vertical and horizontal stubs are set as l_p and l_s, respectively. These two triple-band filters are realized based on the above-discussed principle that two pairs of the first- and third-order degenerate modes are split by the strong line-to-ring coupling under the 135°/45° port-to-port angle, while a pair of second-order degenerate modes are separated relying on proper perturbation of four open-circuited stubs.

Figs. 9(a) and 10(a) show the two complete equivalent-circuit models for the two proposed ring-resonator triple-band filters shown in Fig. 1(a) and (b). In Figs. 9(a) and 10(a), θ_c stands for half the electrical length of the coupled lines, $Z_c = -jZ_{0e}Z_{0o}/[(Z_{0e} + Z_{0o})\tan\theta_c]$, $N = (Z_{0e} + Z_{0o})/(Z_{0e} - Z_{0o})$, and $Z = (Z_{0e} + Z_{0o})/2$, respectively, as studied in [19]. As shown in Figs. 9(b) and 10(b), with no stubs installed, the first and third passbands with two poles in each band are produced, whereas the second passband is fully suppressed by signal cancellation between the upper and lower paths when $2\theta = 135°$ or 45°, i.e., transmission zero. By adding four open-circuited stubs with proper lengths, the second passband is visibly produced with two transmission poles. In this aspect, the first and third passbands slightly drop off due to the slow-wave property of the stub-loaded ring.

In our design, the coupling length (2Φ) and coupling gap (s) of the parallel-coupled lines in Fig. 1(a) and (b) are first determined to achieve the first- and third-order dual-mode passbands under the fixed 135°/45° port excitation angle. Next,

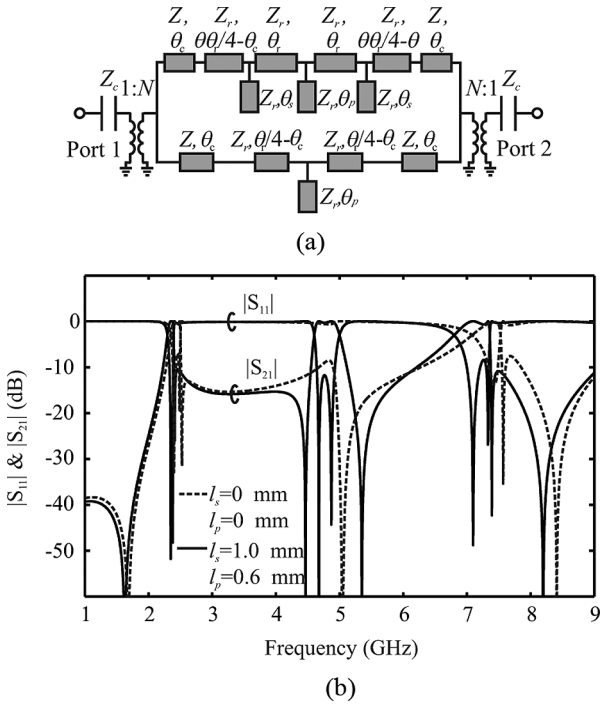

Fig. 10. (a) Equivalent model of the ring circuit in Fig. 1(b). (b) Theoretical frequency responses for varied stub lengths (l_p and l_s) ($r_1 = 7.10$ mm, $r_2 = 7.40$ mm, $w_p = 0.30$ mm, $s = 0.10$ mm, and $\theta_c = 16\theta_r/45$. Substrate: $\epsilon_r = 10.8$, $h = 1.27$ mm).

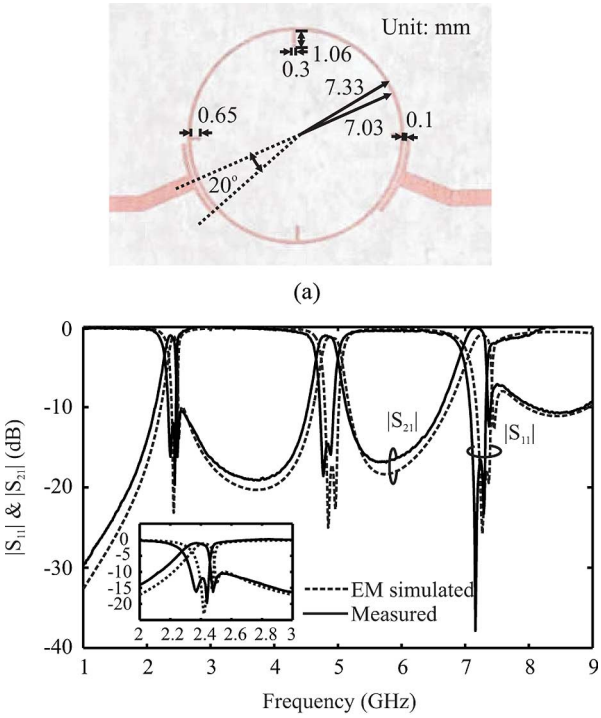

Fig. 11. (a) Photograph of the fabricated filter with 135° port separation. (b) Simulated and measured S_{21} and S_{11} magnitudes.

four open-circuited stubs are attached with the uniform ring at an equally spaced distance to split the second-order degenerate modes, thus making up the second passband with two poles. In order to increase the degree of freedom in controlling the poles in the first and third passbands, the lengths of the two vertical and two horizontal stubs are selected separately. The bandwidth of each passband can be separately adjusted by the odd- and even-mode resonant poles and the coupling strength of the parallel-coupled lines. Looking at Figs. 9(b) and 10(b) together, we can find that the filter in Fig. 10(a) with $2\theta = 45°$ achieves higher filter selectivity out of the triple passbands due to the existence of more transmission zeros. Based on our study in [19], both the first zero at the lower stopband and the second zero at the upper stop are generated by the signal cancellation (out-of-phase principle) from the two paths of the ring resonator. Meanwhile, the two zeros at each side of the second passband are introduced and controlled by the capacitive coupling nature of perturbation.

In order to take into account all the unexpected effects such as frequency dispersion and discontinuities, the two compact dual-mode triple-band bandpass filters are optimally designed using a full-wave electromagnetic (EM) simulator [21]. These two filters are then fabricated on a dielectric substrate with a thickness of 1.27 mm and permittivity of 10.8. Two photographs of the fabricated filters with $2\theta = 135°$ and $45°$ are provided in Figs. 11(a) and 12(a), respectively. Figs. 11(b) and 12(b) indicate the simulated and measured results over a wide frequency range of 1.0–9.0 GHz.

For the first filter with $2\theta = 135°$ in Fig. 11(a), the measured triple passbands are centered at 2.37, 4.83, and 7.31 GHz

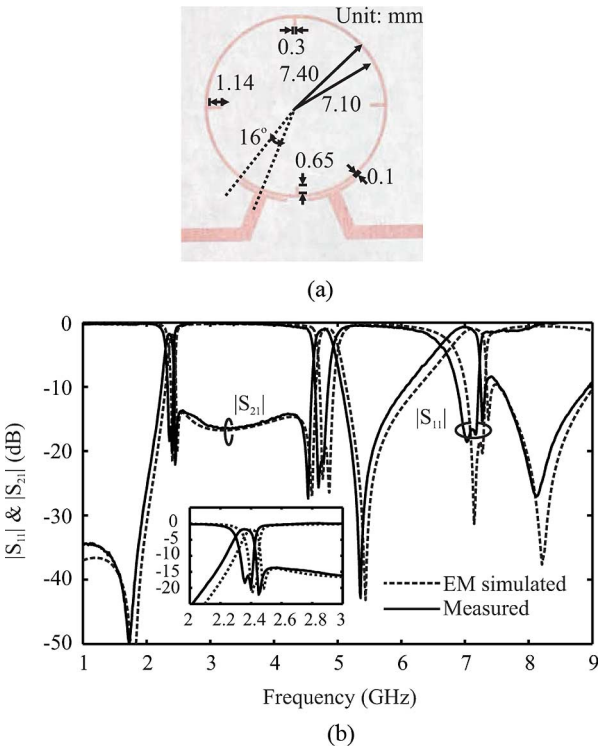

Fig. 12. (a) Photograph of the fabricated filter with 45° port separation. (b) Simulated and measured S_{21} and S_{11} magnitudes.

with the 3-dB fractional bandwidths of 7.1%, 7.1%, and 5.5%, respectively, as can be found from Fig. 11(b). The minimum insertion loss in measurement is equal to about 1.0 dB in the

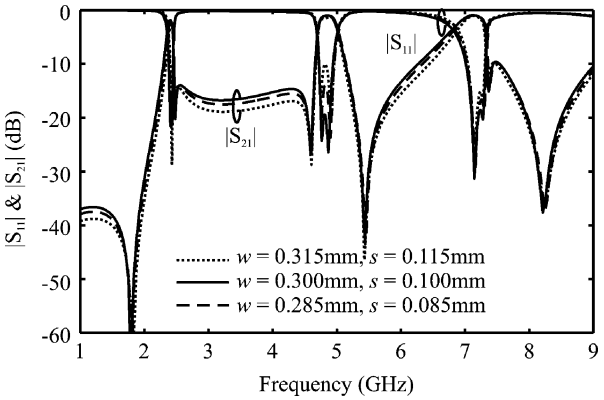

Fig. 13. Three sets of simulated S_{21} and S_{11} magnitudes under different values of strip width of the ring (w) and spacing of the parallel-coupled lines (s).

first/second passbands and 0.6 dB in the third passband. Moreover, the three pairs of measured transmission poles appear at 2.37/2.44, 4.77/4.88, and 7.16/7.29 GHz, as predicted in analysis and simulation, whereas two transmission zeros are created at 2.48 and 7.37 GHz. The attenuation at the lower stopband is better than 10 dB from dc to 2.13 GHz and the attenuation at the upper stopband is better than 7.0 dB from 7.34 to 9.00 GHz. The isolation between the three passbands is better than 10 dB in a range from 2.47 to 4.53 GHz and from 5.13 to 6.63 GHz, respectively.

For the second filter with $2\theta = 45^\circ$ in Fig. 12(a), the measured center frequencies are 2.35, 4.78, and 7.21 GHz with 3-dB fractional bandwidths of 5.31%, 6.27%, and 8.66%, respectively, as can be found from Fig. 12(b). The minimum insertion loss reaches to about 1.78 dB in the first passband, 0.9 dB in the second passband, and 0.7 dB in the third passband. The three pairs of measured poles occur at 2.40/2.36, 4.70/4.78, and 7.02/7.17 GHz. The six transmission zeros are created at 1.73, 2.45, 4.54, 5.35, 7.27, and 8.12 GHz, which have improved the better filter selectivity than that in Fig. 11. At the lower stopband, the attenuation is higher than 34 dB from dc to 1.88 GHz; at the upper stopband, the attenuation is higher than 8.5 dB from 7.2 to 9.0 GHz. The isolation is greater than 14 dB from 2.44 to 4.58 GHz and is greater than 10 dB from 5.07 to 6.10 GHz. In order to verify the sensitivity of the design, three sets of simulated S_{21} and S_{11} magnitudes with the desired values and the extreme values due to the fabrication tolerance $(\pm 0.015$ mm$)$ related to the ring width and the coupling spacing were plotted together in Fig. 13. We can notice from Fig. 13 that positions of the expected transmission zeros and poles are almost unchanged and insertion loss and return loss do not receive any significant influence.

V. Conclusion

In this paper, a novel class of compact dual-mode triple-band bandpass filters based on a single microstrip ring resonator has been presented. In theory, a simple equivalent lumped circuit is presented to provide physical insight into the splitting and movement of the three pairs of odd- and even-mode resonant frequencies with respect to the port excitation angle and four open-circuited stubs. In our analysis and design, the port excitation angle is chosen as 135° and 45° so as to only excite the two pairs of first- and third-order degenerate modes. By properly attaching the four stubs with the ring, a pair of second-order degenerate modes is excited and split, as expected. Finally, two triple-band bandpass filters have been designed and fabricated. Predicted results are verified experimentally, showing the triple passbands with two poles in each passband.

Acknowledgment

The authors would like to thank Dr. A. Do, Nanyang Technological University, Singapore, for his valuable discussion and assistance.

References

[1] Y.-S. Lin, C.-C. Liu, K.-M. Li, and C.-H. Chen, "Design of an LTCC tri-band transceiver module for GPRS mobile applications," *IEEE Trans. Microw. Theory Tech.*, vol. 52, no. 12, pp. 2718–2724, Dec. 2004.

[2] D. L. Kaczman, M. Shah, N. Godambe, M. Alam, H. Guimaraes, L. M. Han, M. Rachedine, D. L. Cashen, W. E. Getka, C. Dozier, W. P. Shepherd, and K. Couglar, "A single-chip tri-band (2100, 1900, 850/800 MHz) WCDMA/HSDPA cellular transceiver," *J. Solid-State Circuits*, vol. 41, no. 5, pp. 1122–1132, May 2006.

[3] C.-H. Lee, C.-I. G. Hsu, and H.-K. Jhuang, "Design of a new tri-band microstrip BPF using combined quarter-wavelength SIRs," *IEEE Microw. Wireless Compon. Lett*, vol. 16, no. 11, pp. 594–596, Nov. 2006.

[4] F.-C. Chen and Q.-X. Chu, "Design of compact tri-band bandpass filters using assembled resonators," *IEEE Trans. Microw. Theory Tech.*, vol. 57, no. 1, pp. 165–171, Jan. 2009.

[5] X. Y. Zhang, Q. Xue, and B. J. Hu, "Planar tri-band bandpass filter with compact size," *IEEE Microw. Wireless Compon. Lett*, vol. 20, no. 5, pp. 262–264, May 2010.

[6] X. Lai, C.-H. Liang, H. Di, and B. Wu, "Design of tri-band filter based on stub loaded resonator and DGS resonator," *IEEE Microw. Wireless Compon. Lett*, vol. 20, no. 5, pp. 265–267, May 2010.

[7] C.-I. G. Hsu, C.-H. Lee, and Y.-H. Hsieh, "Tri-band bandpass filter with sharp passband skirts designed using tri-section SIRs," *IEEE Microw. Wireless Compon. Lett*, vol. 18, no. 1, pp. 19–21, Jan. 2008.

[8] Q.-X. Chu and X.-M. Lin, "Advanced triple-band bandpass filter using tri-section SIR," *Electron. Lett.*, vol. 44, no. 4, pp. 295–296, Feb. 2008.

[9] F.-C. Chen, Q.-X. Chu, and Z.-H. Tu, "Tri-band bandpass filter using stub loaded resonators," *Electron. Lett.*, vol. 44, no. 12, pp. 747–749, Jun. 2008.

[10] Q.-X. Chu, F.-C. Chen, Z.-H. Tu, and H. Wang, "A novel cross resonator and its applications to bandpass filters," *IEEE Trans. Microw. Theory Tech.*, vol. 57, no. 7, pp. 1753–1759, Jul. 2009.

[11] C. Quendo, E. Rius, A. Manchec, Y. Clavet, B. Potelon, J.-F. Favennec, and C. Person, "Planar tri-band filter based on dual behavior resonator (DBR)," in *Proc. Eur. Microw. Conf.*, Oct. 2005, vol. 1, pp. 269–272.

[12] C.-F. Che, T.-Y. Huang, and R.-B. Wu, "Design of dual- and triple-passband filters using alternately cascaded multiband resonators," *IEEE Trans. Microw. Theory Tech.*, vol. 54, no. 9, pp. 3550–3558, Sep. 2006.

[13] M. Mokhtaari, J. Bornemann, K. Rambabu, and S. Amari, "Coupling-matrix design of dual and triple passband filters," *IEEE Trans. Microw. Theory Tech.*, vol. 54, no. 11, pp. 3940–3946, Nov. 2006.

[14] X.-P. Chen, K. Wu, and Z.-L. Li, "Dual-band and triple-band substrate integrated waveguide filters with Chebyshev and quasi-elliptic responses," *IEEE Trans. Microw. Theory Tech.*, vol. 55, no. 12, pp. 2569–2578, Dec. 2007.

[15] J. Lee and K. Sarabandi, "Design of triple-passband microwave filters using frequency transformations," *IEEE Trans. Microw. Theory Tech.*, vol. 56, no. 1, pp. 187–193, Jan. 2008.

[16] B.-J. Chen, T.-M. Shen, and R.-B. Wu, "Design of tri-band filters with improved band allocation," *IEEE Trans. Microw. Theory Tech.*, vol. 57, no. 7, pp. 1790–1797, Jul. 2009.

[17] S. Luo and L. Zhu, "A novel dual-mode dual-band bandpass filter based on a single ring resonator," *IEEE Microw. Wireless Compon. Lett*, vol. 19, no. 8, pp. 497–499, Aug. 2009.

[18] S. Luo, L. Zhu, and S. Sun, "A dual-mode dual-band bandpass filter using a single ring resonator," in *Proc. Asia–Pacific Microw. Conf.*, 2009, pp. 921–924.

[19] S. Luo, L. Zhu, and S. Sun, "A dual-band ring-resonator bandpass filter based on two pairs of degenerate modes," *IEEE Trans. Microw. Theory Tech.*, vol. 58, no. 12, pp. 3427–3432, Dec. 2010.
[20] K. Chang and L. H. Hsieh, *Microstrip Ring Circuit and Related Structures*. New York: Wiley, 2004.
[21] Advanced Design System (ADS) 2006a. Agilent Technol., Palo Alto, CA, 2006.

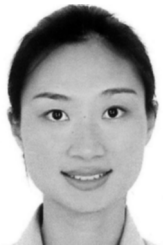

Sha Luo (S'08) was born in Hunan Province, China. She received the B. Eng. degree from Nanyang Technological University (NTU), Singapore, in 2006, and is currently working toward the Ph.D. degree in electrical and electronic engineering at NTU.

From 2006 to 2007, she was a Research Engineer with the Satellite Engineering Communication Laboratory, Singapore. Her research interests include multilayer planar circuits, microwave filters and millimeter-wave passive components.

Ms. Luo was the recipient of the Ministry of Education Scholarship (2002–2006), Singapore and an NTU Research Scholarship (2007–2010).

Lei Zhu (S'91–M'93–SM'00) received the B. Eng. and M. Eng. degrees in radio engineering from the Nanjing Institute of Technology (now Southeast University), Nanjing, China, in 1985 and 1988, respectively, and the Ph.D. Eng. degree in electronic engineering from the University of Electro-Communications, Tokyo, Japan, in 1993.

From 1993 to 1996, he was a Research Engineer with the Matsushita-Kotobuki Electronics Industries Ltd., Tokyo, Japan. From 1996 to 2000, he was a Research Fellow with the École Polytechnique de Montréal, University of Montréal, Montréal, QC, Canada. Since July 2000, he has been an Associate Professor with the School of Electrical and Electronic Engineering, Nanyang Technological University, Singapore. He has authored or coauthored over 200 papers in peer-reviewed journals and conference proceedings, including 20 in the IEEE TRANSACTIONS ON MICROWAVE THEORY AND TECHNIQUES and 35 in the IEEE MICROWAVE AND WIRELESS COMPONENTS LETTERS. His papers have been cited more than 1850 times with the H-index of 23 (source: ISI Web of Science). He was an Associate Editor for the *IEICE Transactions on Electronics* (2003–2005). His research interests include planar filters, planar periodic structures, planar antennas, numerical EM modeling, and deembedding techniques.

Dr. Zhu has been an associate editor for the IEEE MICROWAVE AND WIRELESS COMPONENTS LETTERS since 2006 and an associate editor for the IEEE TRANSACTIONS ON MICROWAVE THEORY AND TECHNIQUES since 2010. He has been a member of the IEEE Microwave Theory and Techniques Society (IEEE MTT-S) Technical Committee 1 on Computer-Aided Design since June 2006. He was a general chair of the 2008 IEEE MTT-S International Microwave Workshop Series (IMWS'08) on Art of Miniaturizing RF and Microwave Passive Components, Chengdu, China, and a Technical Program Committee (TPC) chair of the 2009 Asia–Pacific Microwave Conference (APMC'09), Singapore. He was the recipient of the 1997 Asia–Pacific Microwave Prize Award, the 1996 Silver Award of Excellent Invention from Matsushita–Kotobuki Electronics Industries Ltd., and 1993 First-Order Achievement Award in Science and Technology from the National Education Committee, China.

Sheng Sun (S'02–M'07) received the B.Eng. degree in information and communication engineering from Xi'an Jiaotong University, Xi'an, China, in 2001, and the Ph.D. degree in electrical and electronic engineering from the Nanyang Technological University (NTU), Singapore, in 2006.

From 2005 to 2006, he was with the Integrated Circuits and Systems Laboratory, Institute of Microelectronics, Singapore. From 2006 to 2008, he was with the Department of Electrical and Electronic Engineering, NTU, Singapore. From 2008 to 2010, he was a Humboldt Research Fellow with the Institute of Microwave Techniques, University of Ulm, Ulm, Germany. Since September 2010, he has been a Research Assistant Professor with the Department of Electrical and Electronic Engineering, The University of Hong Kong (HKU), Pokfulam, Hong Kong. His current research interests include EM theory and computational methods, numerical modeling and de-embedding techniques, EM wave propagation and scattering, microwave and millimeter-wave radar system, as well as the study of multilayer planar circuits, microwave filters, and antennas.

Dr. Sun was the recipient of the Outstanding Reviewer Award of the IEEE MICROWAVE AND WIRELESS COMPONENTS LETTERS in 2010, a 2008 Hildegard Maier Research Fellowship of the Alexander von Humboldt Foundation, the Young Scientist Travel Grant of the 2004 International Symposium on Antennas and Propagation, Sendai, Japan, and the 2002–2005 NTU Research Scholarship.